Opto-Electronic Advances

Supplementary information

2022, Vol. 5, No. 5

DOI: 10.29026/oea.2022.210077

Laser additive manufacturing of Si/ZrO_2 tunable crystalline phase 3D nanostructures

Greta Merkininkaitė[1,2], Edvinas Aleksandravičius[3], Mangirdas Malinauskas[3]*, Darius Gailevičius[2,3] and Simas Šakirzanovas[1,4]

[1]Faculty of Chemistry and Geosciences, Vilnius University, Naugarduko Str. 24, Vilnius LT-03225, Lithuania; [2]Femtika, Sauletekio Ave. 15, Vilnius LT-10224, Lithuania; [3]Laser Research Center, Physics Faculty, Vilnius University, Sauletekio Ave. 10, Vilnius LT-10223, Lithuania; [4]Department of Chemical Engineering and Technology, Center for Physical Sciences and Technology, Sauletekio Ave. 3, Vilnius LT-10257, Lithuania.

*Correspondence: M Malinauskas, E-mail: mangirdas.malinauskas@ff.vu.lt

Supplementary information for this paper is available at https://doi.org/10.29026/oea.2022.210077

The FTIR analysis was chosen for the evaluation of chemical changes in prepared sols, gels, and polymers. Characteristic FTIR absorption peaks provide qualitative and semi-quantitative information on hydrolysis, condensation, and polymerization. The broad band absorption at ≈ 3330 cm^{-1} is characteristic of the axial deformation of Si-OH, Zr-OH or C-OH groups, which corresponds solvents, such as methanol and isopropyl alcohol or hydrolyzed silane and zirconium (IV) propoxide in sols (Fig. S1(a)). It is clear that during condensation (the process described in the paragraph "Materials and Synthesis") solvents, such as methanol and isopropyl alcohol are removed from materials, therefore, a band of -OH groups (≈ 3330 cm^{-1}) decreases in gels and polymers spectra. Similar conclusions can be made for gels (Fig. S1(b)), FTIR spectra show the condensation reaction progress during which various Si-O-Si, Zr-O-Zr and Si-O-Zr bonds are formed. After condensation (Fig. S1(b)) Si-O-Si (1130–1000 cm^{-1}), Si-O-Zr (1000–900 cm^{-1}), Zr-O-Zr ($^{-1}$) absorption become broader and more complex, showing more overlapping bands, which confirms that siloxanes, silanolates or zircoxanes chains become longer or branched. Additionally, FTIR data (Fig. S1(c)) indicate polymerization reaction process during which the signal of alkene groups diminishes, leading to polymerized material after thermal treatment for 3 hours at 140 °C

Refractive indices of prepared sols and gels are depicted in Fig. S2. It can be concluded that zirconium content increase raises the refractive index in both sols and gels. However, the change in refractive indices for different composition gels is small enough that there is no need for additional equipment adjustment during the fabrication process. Based on refractive index tendencies for sol and gels, it can be assumed that obtained polymers will follow a similar trend, i. e. slight increase in index values. Polymeric materials that have a greater refractive index than 1.50 are attributed to high-refractive-index polymers (HRIP), which on their own find applications in various fields[1,2]. For the most part, the refractive indices of all prepared materials in this study are greater than 1.50 (except Si9:Zr1).

The surface quality of ceramic structures annealed at 1400 °C is clearly seen in Fig. S3. The porosity and deformations of the structure are observed only in the skeleton made of Si9:Zr1 (Fig. S3(f, k)). Unfortunately, corner fractures of the structures occurred by placing them on the carbon film prior to SEM analysis.

In order to determine the resistance of ceramic structures to negative temperatures, the study described below was performed. A corundum substrate with Si9:Zr1 3D ceramic nanostructures on the surface was instantly immersed in a thermos filled with liquid nitrogen (≈77 K) and stored until the nitrogen had completely evaporated under ambient conditions. The evaporation process lasted 10 minutes. The results of this study confirmed that such structures remain

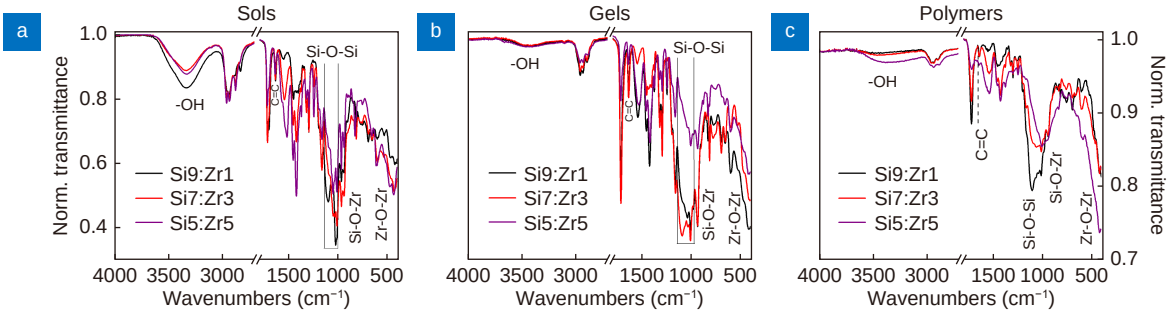

Fig. S1 | Fourier transform infrared spectroscopy (FTIR) spectra of Si_X:Zr_Y sols (**a**), gels (**b**) and polymers (**c**).

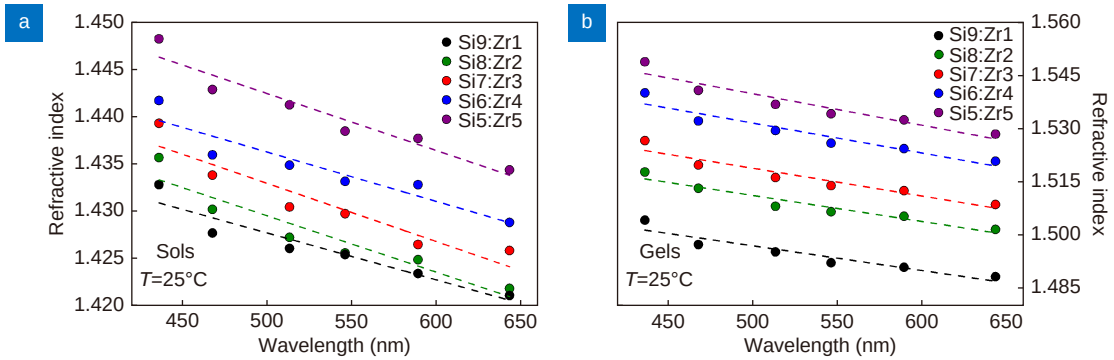

Fig. S2 | Refractive indices (*n*) of Si_X:Zr_Y materials at room temperature (sols (**a**) and gels (**b**)) as a function of wavelength. Each measurement was repeated three times, estimated standard deviations were negligible

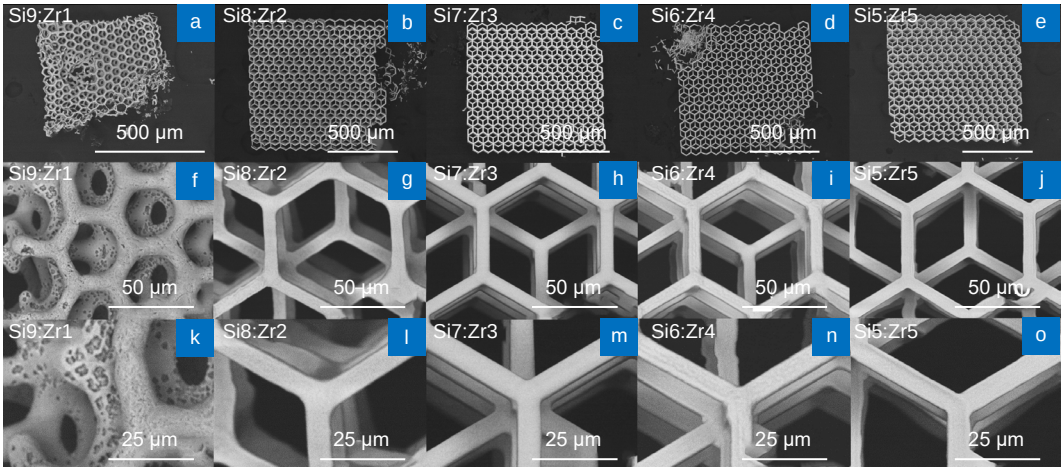

Fig. S3 | Scanning electron microscope images of Si9:Zr1 (**a**, **f**, **k**), Si8:Zr2 (**b**, **g**, **l**), Si7:Zr3 (**c**, **h**, **m**), Si6:Zr4 (**d**, **i**, **n**), Si5:Zr5(**e**, **j**, **o**) skeletons annealed at 1400 °C. The scale bars are 500 (a–e), 50 (f–j) and 25 μm (k–o)

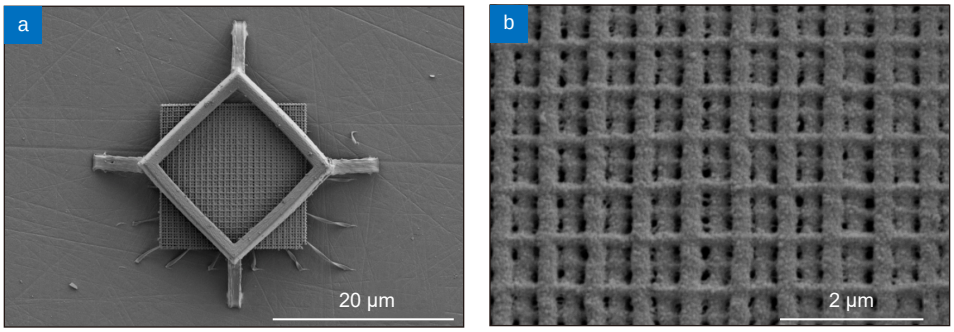

Fig. S4 | Scanning electron microscope images of Si9:Zr1ceramic woodpile fabricated at 500 μm/s and 64 μW after storage in liquid nitrogen (~77 K) for 10 minutes. The scale bars are 20 μm (**a**) and 2 μm (**b**). The surface grainy structure is due to a magnetron sputtered conductive 10-20 nm metallic silver to reduce the charge up during SEM observations.

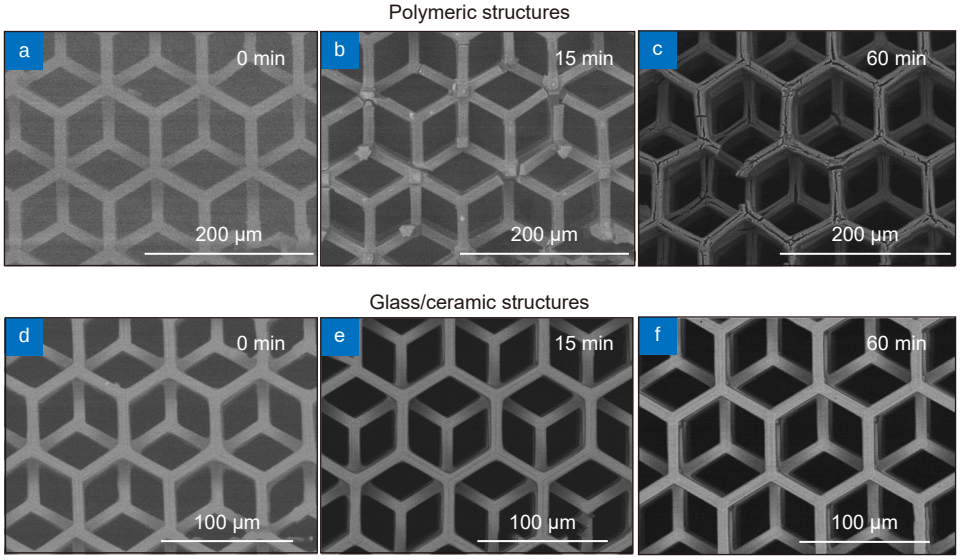

Fig. S5 | Chemical resistance investigation - applying ultrasonic bath while immersion in piranha solution. (**a**) Si7:Zr3 polymeric structure before chemical treatment. (**b**) Si7:Zr3 polymeric structure after chemical treatment (duration 15 min). (**c**) Si7:Zr3 polymeric structure after chemical treatment (duration 60 min). (**d**) Si7:Zr3 ceramic structure (after 1000 °C heat treatment) before chemical treatment. (**e**) Si7:Zr3 ceramic structure after chemical treatment (duration 15 min). (**f**) Si7:Zr3 ceramic structure after chemical treatment (duration 60 min).

robust and the adhesion between the specimen and the substrate remains even after the rapid negative temperature impact. According to SEM measurements of Si9:Zr1 ceramic woodpile fabricated at 500 μm/s and 64 μW (see Fig. S4), the negative temperature caused no damage to the 3D nanostructures or their detachment from the substrate (which, intuitively, could be caused due to different thermal expansion coefficients).

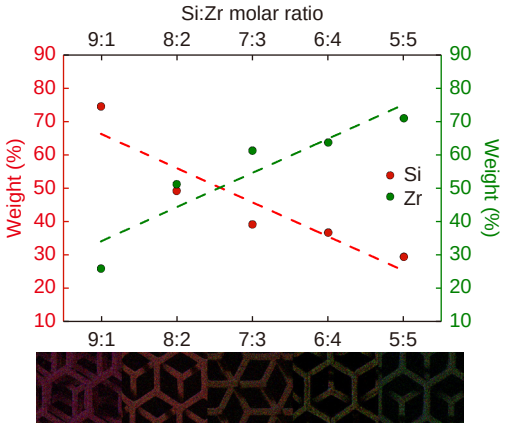

Fig. S6 | Energy-dispersive X-ray spectroscopy (EDS) analysis of scaffolds annealed at 1000 °C. The graph above shows the elements weight (w%) dependence on the initial composition of materials. Images below- EDS mapping of skeleton, where Si-red, Zr-green.

For the resistance study of ceramic structures to aggressive chemical impact, ceramic (annealed at 1000 °C) in a comparison with polymeric Si7:Zr3 scaffolds were processed in a solution of piranha (volume ratio of 4:1 sulfuric acid (Chempur, 95–98%) and peroxide (Chempur, 50%)), a highly corrosive and an extremely powerful oxidizer, in an ultrasonic bath for 15 and 60 minutes, respectively. The polymeric skeleton cracked and acquired defects after piranha and ultrasonic treatment (Fig. S5(b, c)), while the ceramic structure showed complete immunity to aggressive conditions (Fig. S5(e, f)).

The graph in Fig. 6 shows the dependence of the mass of silicon and zirconium elements on the initial sols composition. The images below are EDX maps of the spatial distributions of elements. Energy dispersive X-ray analysis confirmed that during photopolymerization and heating processes the relative amount of silicon and zirconium does not change and elements are evenly distributed over the entire surface of inorganic structures.

In order to compare obtained experimental results to the theoretical predictions, the theoretical shrinkage was calculated. The mass and density of each material was calculated using molecular weights of fully condensed precursors and methacrylic acid (molecular weights: condensed ZPO- 91.22 g/mol, condensed MAPTMS- 155.25 g/mol, MAA- 86.09 g/mol and oxygen- 15.999 g/mol), (densities: ZPO- 1.058 g/cm^3, MAPTMS- 1.045 g/cm^3, MAA- 1.020 g/cm^3). The expected mass and density of ceramics was calculated based on assumption that silicon and zirconium are completely transformed to cristobalite and tetragonal ZrO_2 (molecular weights: cristobalite- 60.08 g/mol, t-ZrO_2- 123.22 g/mol), (densities: cristobalite (COD 96-900-8226)- 2.309 g/cm$_2$, t-ZrO_2 (COD 96-152-5706)- 6.190 g/cm$_2$).

Table S1 | Volume of cubes and volumetric shrinkage after heating.

Volume of cubes before heating								
Sample	a_1 (μm)	a_2 (μm)	a_3 (μm)	V_1 (μm^3)	V_2 (μm^3)	V_3 (μm^3)	$V_{avg.}$ (μm^3)	Std. dev. (μm^3)
Si9:Zr1	23.60	23.82	22.33	13147	13517	11128	12598	1286
Si8:Zr2	25.45	24.83	24.95	16476	15303	15535	15771	621
Si7:Zr3	23.56	23.14	23.30	13078	12389	12649	12705	348
Si6:Zr4	21.03	21.98	23.54	9299	10616	13036	10984	1895
Si5:Zr5	23.38	23.37	23.27	12778	12770	12601	12717	100
Volume of cubes after heating								
Sample	a_1 (μm)	a_2 (μm)	a_3 (μm)	V_1 (μm^3)	V_2 (μm^3)	V_3 (μm^3)	$V_{avg.}$ (μm^3)	Std. dev. (μm^3)
Si9:Zr1	14.30	14.18	14.03	2921	2851	2763	2845	79
Si8:Zr2	15.93	15.72	15.57	4060	3885	3776	3907	143
Si7:Zr3	14.41	14.76	14.66	2992	3218	3147	3119	116
Si6:Zr4	14.58	14.07	15.88	3101	2785	4001	3296	631
Si5:Zr5	15.48	16.35	15.82	3707	4372	3956	4012	336
Volumetric shrinkage								
Sample	$\Delta V_{1(Shrinkage)}$(%)		$\Delta V_{2(Shrinkage)}$(%)		$\Delta V_{3(Shrinkage)}$(%)		$\Delta V_{avg.(Shrinkage)}$(%)	Std. dev.(%)
Si9:Zr1	77.78		78.91		75.16		77.28	1.92
Si8:Zr2	75.36		74.6		75.69		75.69	0.56
Si7:Zr3	77.12		74.02		75.12		75.42	2.19
Si6:Zr4	66.66		73.76		69.31		75.57	3.58
Si5:Zr5	70.99		65.76		68.6		68.45	3.69

Table S2 | Width of woodpiles lines before heating.

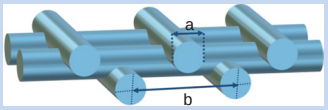

Si9:Zr1						
Velocity (μm/s)	Power (μW)	a_1 (nm)	a_2 (nm)	a_3 (nm)	$a_{avg.}$ (nm)	Std. dev. (nm)
200	48	190	169	188	182	11.6
200	56	157	187	207	184	25.2
200	64	99	109	129	112	15.3
500	48	208	238	238	228	17.3
500	56	206	222	202	210	10.6
500	64	178	188	208	191	15.3
Si8:Zr2						
200	48	286	307	317	303	15.8
200	56	298	288	302	296	7.2
200	64	258	280	290	276	16.4
500	48	247	246	256	250	5.5
500	56	250	295	284	276	23.5
500	64	228	262	232	241	18.6
Si7:Zr3						
200	48	277	280	271	276	4.6
200	56	287	278	267	277	10.0
200	64	209	276	251	245	33.8
500	48	222	216	214	217	4.2
500	56	223	225	238	229	8.1
500	64	272	287	278	279	7.6
Si6:Zr4						
200	48	208	206	199	204	4.7
200	56	251	249	233	244	9.9
200	64	208	219	188	205	15.7
500	48	234	252	266	251	16.0
500	56	178	192	201	190	11.6
500	64	258	277	264	266	9.7
Si5:Zr5						
200	48	263	279	279	274	9.2
200	56	316	343	317	325	15.3
200	64	278	265	286	276	10.6
500	48	207	206	191	201	9.0
500	56	239	223	230	231	8.0
500	64	222	262	246	243	20.1

Table S3 | Width of woodpiles periods before heating.

Si9:Zr1						
Velocity (μm/s)	Power (μW)	b_1 (nm)	b_2 (nm)	b_3 (nm)	$b_{avg.}$ (nm)	Std. dev. (nm)
200	48	818	858	839	838	20.0
200	56	915	905	876	899	20.3
200	64	881	882	906	890	14.2
500	48	891	931	891	904	23.1
500	56	921	913	929	921	8.0
500	64	937	923	947	936	12.1
Si8:Zr2						
200	48	971	990	961	974	14.7
200	56	949	960	969	959	10.0
200	64	1011	961	991	988	25.2
500	48	980	901	970	950	43.0
500	56	1000	1040	1003	1014	22.3
500	64	956	975	956	962	11.0
Si7:Zr3						
200	48	961	951	980	964	14.7
200	56	951	921	970	947	24.7
200	64	941	936	941	939	2.9
500	48	953	959	982	965	15.3
500	56	921	948	961	943	20.4
500	64	870	871	817	853	30.9
Si6:Zr4						
200	48	822	852	832	835	15.3
200	56	847	858	821	842	19.0
200	64	862	852	832	849	15.3
500	48	840	867	841	849	15.3
500	56	892	891	861	881	17.6
500	64	856	886	857	866	17.0
Si5:Zr5						
200	48	951	931	961	948	15.3
200	56	881	861	891	878	15.3
200	64	881	905	897	894	12.2
500	48	913	900	926	913	13.0
500	56	883	873	847	868	18.6
500	64	872	842	832	849	20.8

Table S4 | Width of woodpiles lines after heating at 1000 ℃ under air atmosphere.

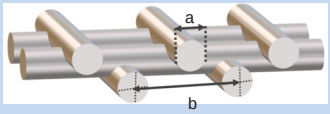

Velocity (μm/s)	Power (μW)	a_1 (nm)	a_2 (nm)	a_3 (nm)	$a_{avg.}$ (nm)	Std. dev. (nm)
Si9:Zr1						
200	48	135	141	147	141	6.0
200	56	139	143	155	146	8.3
200	64	60	57	59	58.7	1.5
500	48	190	206	186	194	10.6
500	56	183	199	175	186	12.2
500	64	185	172	159	172	13.0
Si8:Zr2						
200	48	258	262	247	256	7.8
200	56	236	237	235	236	1.0
200	64	227	238	248	238	10.5
500	48	167	157	165	163	5.3
500	56	206	185	173	188	16.7
500	64	176	186	191	184	7.6
Si7:Zr3						
200	48	216	212	234	221	11.7
200	56	208	218	204	210	7.2
200	64	197	185	173	185	12.0
500	48	151	135	167	151	16.0
500	56	169	184	192	182	11.7
500	64	225	172	185	194	27.6
Si6:Zr4						
200	48	176	182	186	181	5.0
200	56	150	170	173	164	12.5
200	64	166	149	151	155	9.3
500	48	197	182	187	189	7.6
500	56	161	166	168	165	3.6
500	64	207	217	227	217	10.0
Si5:Zr5						
200	48	173	180	169	174	5.6
200	56	213	193	213	206	11.5
200	64	196	185	190	190	5.5
500	48	148	160	152	153	6.1
500	56	139	164	156	153	12.8
500	64	169	175	191	178	11.4

Table S5 | Width of woodpiles periods after heating at 1000 ℃ under air atmosphere.

Si9:Zr1						
Velocity (μm/s)	Power (μW)	b_1 (nm)	b_2 (nm)	b_3 (nm)	$b_{avg.}$ (nm)	Std. dev. (nm)
200	48	651	643	651	648	4.6
200	56	662	665	630	652	19.4
200	64	622	625	667	638	25.2
500	48	611	627	667	635	28.8
500	56	643	643	627	637.7	9.2
500	64	667	651	675	664	12.2
Si8:Zr2						
200	48	699	651	699	683	27.7
200	56	676	658	649	661	73.7
200	64	634	624	624	627	5.8
500	48	651	619	635	635	16.0
500	56	651	668	635	651	16.5
500	64	627	659	627	638	18.5
Si7:Zr3						
200	48	570	850	545	565	18.0
200	56	548	518	538	535	15.3
200	64	572	603	584	58	15.6
500	48	562	573	541	559	16.3
500	56	540	564	524	543	20.1
500	64	515	520	516	517	2.6
Si6:Zr4						
200	48	555	527	526	536	16.5
200	56	522	543	536	534	10.7
200	64	551	516	529	532	17.7
500	48	574	576	545	565	17.3
500	56	549	559	542	550	8.5
500	64	571	552	562	562	9.5
Si5:Zr5						
200	48	555	529	528	537	15.3
200	56	518	539	512	523	14.2
200	64	513	518	515	515	2.5
500	48	523	579	605	569	41.9
500	56	521	543	586	550	33.1
500	64	567	523	550	547	22.2

References

1. Liu JG, Ueda M. High refractive index polymers: fundamental research and practical applications. *J Mater Chem* **19**, 8907–8919 (2009).
2. Macdonald EK, Shaver MP. Intrinsic high refractive index polymers. *Polym Int* **64**, 6–14 (2015).